Published in final edited form as:
Macromolecules. 2013 August 13; 46(15): 6319–6325. doi:10.1021/ma4007544.

Structural characterization of amphiphilic homopolymer micelles using light scattering, SANS, and cryo-TEM

Joseph P. Patterson[a,‡], **Elizabeth G. Kelley**[b,‡], **Ryan P. Murphy**[b], **Adam O. Moughton**[a], **Mathew Robin**[a], **Annhelen Lu**[a], **Olivier Colombani**[c], **Christophe Chassenieux**[c], **David Cheung**[a,§], **Millicent O. Sullivan**[b], **Thomas H. Epps III**[b], and **Rachel K. O'Reilly**[a]

Thomas H. Epps: thepps@udel.edu; Rachel K. O'Reilly: r.k.o-reilly@warwick.ac.uk

[a]University of Warwick, Department of Chemistry, Gibbet Hill Road, Coventry, CV4 7AL, United Kingdom

[b]University of Delaware, Department of Chemical and Biomolecular Engineering, 150 Academy Street, Newark, DE 19716, United States

[c]LUNAM Université, Université du Maine, IMMM UMR CNRS 6283, Département PCI, Avenue Olivier Messiaen, 72085 Le Mans Cedex 09, France

Abstract

We report the aqueous solution self-assembly of a series of poly(N-isopropylacrylamide) (PNIPAM) polymers end-functionalized with a hydrophobic sulfur-carbon-sulfur (SCS) pincer ligand. Although the hydrophobic ligand accounted for <5 wt% of the overall homopolymer mass, the polymers self-assembled into well-defined spherical micelles in aqueous solution, and these micelles are potential precursors to solution-assembled nanoreactors for small molecule catalysis applications. The micelle structural details were investigated using light scattering, cryogenic transmission electron microscopy (cryo-TEM), and small angle neutron scattering (SANS). Radial density profiles extracted from the cryo-TEM micrographs suggested that the PNIPAM chains formed a diffuse corona with a radially decreasing corona density profile and provided valuable *a priori* information about the micelle structure for SANS data modeling. SANS analysis indicated a similar profile in which the corona surrounded a small hydrophobic core containing the pincer ligand. The similarity between the SANS and cryo-TEM results demonstrated that detailed information about the micelle density profile can be obtained directly from cryo-TEM and highlighted the complementary use of scattering and cryo-TEM in the structural characterization of solution-assemblies, such as the SCS pincer-functionalized homopolymers described here.

Introduction

In recent decades, the solution self-assembly of amphiphilic block copolymers (BCP)s has attracted significant attention given the utility of BCPs in a variety of applications, including

Correspondence to: Thomas H. Epps, III, thepps@udel.edu; Rachel K. O'Reilly, r.k.o-reilly@warwick.ac.uk.

§**Present Address:** Department of Pure and Applied Chemistry, University of Strathclyde, Glasgow, G1 1XL, UK.

‡ **Author Contributions:** J.P.P and E.G.K contributed equally to this work.

Notes

The authors declare no competing financial interest.

Supporting Information

CMC fluorescence data (Figure S1); additional light scattering data (Figure S2 through S6); additional cryo-TEM images (Figure S7); detailed explanation of cryo-TEM micrograph analysis; SANS data model; details of molecular simulations (Table S1, Table S2, and Figure S8); calculated corona chain stretching (Table S3). This material is available free of charge via the Internet at http://pubs.acs.org.

drug and gene delivery systems,[1, 2] nanoreactors in separation science,[3] and nanoelectronics.[4] The solution self-assembly of another class of amphiphiles, so-called 'associative polymers' or 'amphiphilic homopolymers', also has been studied extensively.[5-26] Examples of these systems include homopolymers in which the monomer units contain both hydrophilic and hydrophobic moieties[6-8] or homopolymers end-functionalized with ionic head groups[12] or small hydrophobic groups, such as alkyl chains.[8, 10, 11, 14, 16, 17, 23-25] Like amphiphilic diblock or triblock copolymers, these amphiphilic homopolymers have been shown to self-assemble into well-defined structures, making them promising materials for applications that necessitate aqueous solution-assembly.[10,22]

Recent advances in controlled radical polymerization methods, such as reversible addition-fragmentation chain transfer (RAFT), have facilitated the incorporation of hydrophobic end-groups onto polymer chains.[10, 11, 22] Incorporating hydrophobic groups on RAFT chain transfer agents (CTA)s is a convenient means of synthesizing amphiphilic homopolymers with controlled molecular weights, low dispersities (Đ), and high end-group fidelity.[27, 28] Furthermore, careful design of hydrophobic end-groups not only facilitates self-assembly but also incorporates reactive centers for potential catalysis applications. There is significant interest in developing aqueous nanoreactors given their potential to improve catalyst efficiency as well as simplify product and catalyst recovery.[29-31] We recently incorporated a sulfur-carbon-sulfur (SCS) pincer ligand into a RAFT agent, allowing for simple access to a variety of polymer structures for catalysis applications.[32] We showed that by using aqueous nanoreactors formed from poly(acrylic acid) hompolymers end-functionalized with a Pd pincer end-group, we were able to create hydrophobic nanopockets to increase the activity of a Pd catalyzed coupling reaction.[32] However, these amphiphilic homopolymers formed a mixture of spherical and cylindrical micelles, making detailed analysis of the nanostructures (through small angle scattering and electron microscopy methods) difficult.

Cryogenic transmission electron microscopy (cryo-TEM) is a powerful tool for characterizing solution-assembled nanostructures and has provided unique insights into nanoscale morphologies as well as self-assembly processes and phase transition behavior.[33-35] While cryo-TEM is used throughout literature to study solution assembled structures,[33-35] fewer reports have demonstrated the utility of this technique for analyzing the radial density distribution of polymeric nanoparticles.[36-38] The detailed density distribution of nanostructures is investigated more often using small angle neutron or X-ray scattering (SANS or SAXS) experiments.[36, 39-42] However, as highlighted by Ballauff *et al.*, both cryo-TEM and small angle scattering methods are sensitive to the local density distribution of the sample.[36] By using both SAXS and cryo-TEM micrograph analysis, Ballauff *et al.* showed that quantitative structural information can be determined from cryo-TEM micrographs of colloidal particles.[36] Herein, we use a similar approach and exploit both cryo-TEM micrograph analysis and SANS experiments to study the solution-assembled structure of amphiphilic homopolymers.

We report the preparation of a series of poly(N-isopropylacrylamide) homopolymers functionalized with an SCS pincer ligand using RAFT and the detailed study of the solution assembly behavior of these homopolymer amphiphiles using a combination of scattering techniques and cryo-TEM. Importantly, these pincer-functionalized amphiphilic homopolymers are potential precursors to solution-assembled nanoreactors exhibiting catalytic activity. The current work focuses on characterizing the aqueous solution assembly of pincer-functionalized homopolymers with different molecular weights, as the ability to understand and tailor the self-assembly of these materials will allow for more detailed studies of the effects of nanoreactor nanostructure on catalytic properties.

Experimental Section

Materials

All chemicals were used as received from Aldrich, Fluka, or Acros unless otherwise stated. AIBN (azobisisobutyronitrile) was recrystallized twice from methanol[43] and stored in the dark at 5 °C. SCS pincer CTA was synthesized as reported previously.[32]

General procedure of RAFT polymerization of N-isopropylacrylamide (NIPAM)—SCS pincer CTA (0.050 g, 57 mol), NIPAM (1.3 g, 12 mmol), AIBN (2.8 mg, 17 mol), and dimethylformamide (DMF) (2.7 mL) were added to a clean, dry ampoule under N_2 (g). The solution was degassed via 3 freeze-pump-thaw cycles and heated to 65 °C for 5 h under N_2 (g). The viscous crude reaction medium was dissolved in the minimum amount of tetrahydrofuran (THF), and the polymer was precipitated into diethyl ether and filtered. The precipitation process was repeated, and 1.35 g of yellow polymer was recovered. M_n^{NMR} (21.3 kDa), M_n^{GPC} (20.2 kDa), M_w/M_n^{GPC} (1.22). ^{1}H NMR 400MHz ($CDCl_3$): δ (ppm) 7.19 (s, 1H, Ar-*H*), 7.14 (s, 2H, Ar-*H*), 5.70-7.50 (br, N*H*, polymer), 5.05 (s, 2H, Ar-CH_2O), 4.00 (s, br, N(CH_3)$_2$C*H*, 180H, polymer), 3.68 (s, 4H, SCH_2-Ar), 3.33 (t, J = 7.6 Hz, 2H, SCSCH_2C), 2.39 (t, J = 7.4 Hz, 4H, $CH_2SCH_2CH_2$), 1.2-2.5 (br, CH, CH_2, CH_3 polymer).

General procedure for end group removal—PNIPAM (1.1 g, 72 μmol), AIBN (5.0 mg, 29 μmol), 1-ethylpiperidine hypophosphite (EPHP) (0.065 g, 0.36 mmol), and toluene (ca 10 mL) were added to a clean, dry ampoule under N_2 (g). The reaction vessel was degassed via 5 freeze-pump-thaw cycles. The ampoule was filled with N_2 (g) and heated to ~100 °C for 12 h. All volatiles were removed *in vacuo*, the white solid was dissolved in the minimum volume of THF, and the polymer was precipitated into hexanes. 0.79 g of white polymer was recovered. For additional purification, the polymer was dialyzed against deionized water. M_n^{NMR} (21.0 kDa), M_n^{GPC} (20.3 kDa), M_w/M_n^{GPC} (1.22). ^{1}H NMR 400MHz ($CDCl_3$): δ (ppm) 7.19 (s, 1H, Ar H), 7.14 (s, 2H, Ar H), 5.70-7.50 (br, NH, polymer), 5.05 (s, 2H, PhCH_2O), 4.00 (N(CH_3)$_2$CH, 180H, polymer), 3.68 (s, 4H, SCH_2Ph), 2.39 (t, J = 7.4 Hz, 4H, $CH_2SCH_2CH_2$), 1.2-2.5 (br, CH, CH_2, CH_3 polymer).

Polymer characterization

Proton nuclear magnetic resonance spectroscopy (^{1}H NMR)—^{1}H NMR spectra were recorded on a Bruker DPX-400 spectrometer in $CDCl_3$. Chemical shifts are given in ppm downfield from tetramethylsilane (TMS). The degree of polymerization (N_{PNIPAM}) was determined by comparing the integration of the end group peaks (δ 5.05, 3.68 and 3.33) to the C*H* peak (δ 4.00) of the polymer backbone. The number average molecular weight from NMR was calculated according to $M_n = N_{PNIPAM} * M_o + M_{pincer}$, in which M_o is the repeat unit molecular weight of PNIPAM, and M_{pincer} is the end-group molecular weight.

Size exclusion chromatography (SEC)—SEC measurements were conducted on a system comprised of a Varian 390-LC-Multi detector suite fitted with differential refractive index (DRI), and ultra-violet (UV) detectors, and equipped with a guard column (Varian Polymer Laboratories PLGel 5 M, 50 × 7.5 mm) and two mixed D columns (Varian Polymer Laboratories PLGel 5 μM, 300 × 7.5 mm). The mobile phase was THF with 5 vol% triethylamine at a flow rate of 1.0 mL min^{-1}, and samples were calibrated against Varian Polymer Laboratories Easi-Vials linear poly(methyl methacrylate) standards using Cirrus v3.3 software.

Fourier Transform Infrared Spectroscopy (FT-IR)—FT-IR spectra were recorded using a Perkin-Elmer Spectrum 100 FT-IR spectrometer.

Micelle preparation

Micelle solutions were prepared by adding H_2O to the dried polymer powder and stirring overnight. The resulting solutions were filtered through a 0.45 μm nylon filter.

Micelle characterization

Light Scattering (LS)—Static light scattering (SLS) and dynamic light scattering (DLS) measurements were performed on a ALV CGS3 spectrometer operating at λ = 632.8 nm. All LS data were collected at 25 °C.

SLS and DLS data were recorded simultaneously for each system. Measurements were made at 4 different concentrations ranging from 1.0 mg mL^{-1} to 10 mg mL^{-1} and 5 different angles (θ) ranging from 30° to 140°. The scattering vector was defined as $q = 4\pi n/\lambda \sin(\theta/2)$, in which n is the refractive index of the solvent. The scattered intensity was measured over a period of 100 s to determine both the intensity auto correlation function, $g_2(t)$, from DLS and the mean scattered intensity, I, from SLS. For DLS data, the measured $g_2(t)$ was related to the electric field auto correlation function, $g_1(t)$, using the Siegert relation.[44] The resulting functions were analyzed using the REPES routine[45] assuming a continuous distribution of relaxation times, $A(\log(\tau))$, according to Equation 1. The difference between the measured and calculated baseline for the DLS correlation functions was less than 0.1%.

$$g_1(log(t)) = \int_0^\infty \tau A(\tau) exp\left(-\frac{t}{\tau}\right) d\ log\ \tau \quad (1)$$

For many of the samples, the resulting distribution of relaxation times was bimodal. Both the fast (τ_{fast}) and slow (τ_{slow}) relaxation times were q^2-dependent (Figure S2), indicating that diffusive motions were probed. The apparent diffusion coefficient was calculated using the relation $D_i = (q^2\tau_i)^{-1}$, in which i denotes fast or slow. The diffusion coefficient was extrapolated to zero concentration (Figure S3) and was used to calculate the hydrodynamic radii (R_H) for the fast relaxation mode according to the Stokes-Einstein equation.

For SLS experiments, both the slow and fast modes of relaxation contributed to the total scattered intensity. The Rayleigh ratio for the fast mode ($R_{\theta,\ fast}$) of relaxation was calculated according to Equation 2,

$$R_{\theta,fast} = A_{fast}(\theta) R_\theta = A_{fast}(\theta) \frac{I_{sample}(\theta) - I_{solvent}(\theta)}{I_{reference}(\theta)} R_{reference} \quad (2)$$

in which $A_{fast}(\theta)$ is the scattered intensity contribution from the fast mode of relaxation at a given scattering angle determined by DLS (Equation 1), I_{sample}, $I_{solvent}$, and $I_{reference}$ are the scattered intensities at angle θ, by the sample, solvent, and reference liquid, respectively, and $R_{reference}$ is the Rayleigh ratio for the reference liquid. Toluene was used as the reference.

Assuming the concentration of species contributing to the fast mode of relaxation was equal to the polymer concentration in solution (i.e. negligible concentration of larger species, see text for discussion), the weight-average molecular weight (M_w), second virial coefficient (A_2), and radius of gyration (R_g) were estimated according to,

$$\frac{Kc}{R_{\theta,fast}} = \frac{1}{M_w}\left(1 + \frac{q^2 {R_g}^2}{3}\right) + 2A_2 c \quad (3)$$

in which c is the solution concentration and K is a constant, given by Equation 4.

$$K = \frac{4\pi^2 n_{ref}^2 (d\,n/d\,c)^2}{\lambda^4 N_A} \quad (4)$$

In Equation 4, n_{ref} is the refractive index of the reference liquid, dn/dc is the refractive index increment of the polymer, and N_A is Avogadro's number. The dn/dc values were 0.12 (for each polymer) at 25 °C, as determined using a refractometer (Bischoff RI detector) with a laser wavelength of 532 nm.

$Kc/R_{\theta,fast}$ was independent of q^2 (Figure S4), therefore $Kc/R_{\theta,fast}$ values were averaged for all angles and plotted versus concentration to determine the M_w and A_2 (Figure S5). The reported error for all light scattering results was 10% of the average.

Cryogenic transmission electron microscopy (cryo-TEM)—Micelle solutions for cryo-TEM experiments were prepared at concentrations ranging from 2.0 mg mL^{-1} to 5.0 mg mL^{-1}. Samples for cryo-TEM were prepared at 25 °C in a constant humidity environment using a FEI 110 Vitrobot. A 2 -10 μL droplet of micelle solution was applied to a holey carbon-coated copper grid, and the grid was blotted to remove excess solution. Subsequently, the sample was vitrified by plunging the grid into liquid ethane. Grids were transferred to a Gatan cryo stage and imaged using a Tecnai G2 12 Twin TEM at an accelerating voltage of 120 kV. The temperature of the cryo stage was maintained below -170 °C.

The radial gray values, $G(r)$, from the cryo-TEM micrographs were determined in ImageJ,[46] and the profiles were fit according to

$$\frac{G(r)}{G_0} = exp\left(-2K\rho_{corona}(r)\sqrt{R^2 - r^2}\right) \quad (5)$$

in which G_0 is the background gray value, K is a fitting constant, $\rho_{corona}(r)$ is the density distribution of polymer in the micelle corona, R is the micelle radius, and r is the distance from the center of the micelle.[36] The density distribution, $\rho_{corona}(r)$, was modeled as the linear combination of 2 b splines.[41, 42] Additional details pertaining to the cryo-TEM micrograph analysis are provided in the Supporting Information.

Small angle neutron scattering (SANS)—Solutions for SANS experiments were prepared at a concentration of 2.0 mg mL^{-1} by direct dissolution of the polymer powder in D_2O and then filtered using a 0.2 μm nylon filter. All micelle solutions were dried to determine the exact concentration after completion of the SANS experiments.

SANS experiments were performed at the National Institute of Standards and Technology (NIST), Center for Neutron Research (NCNR, Gaithersburg, MD) on the NG-7 30 m SANS beamline. An incident wavelength of 6.0 Å with a wavelength spread ($\Delta\lambda/\lambda$) of 0.12 was used with sample to detector distances of 1.0 m, 4.0 m, and 13.5 m to access a scattering vector (q) range of 0.004 $Å^{-1} < q < 0.6$ $Å^{-1}$. Here, the scattering vector is defined as $q = 4\pi/\lambda \sin(\theta/2)$, in which θ is the scattering angle. All measurements were performed at ambient temperature (20 ± 1 °C). SANS data were reduced using standard procedures provided by NIST,[47] and background scattering from D_2O was subtracted from the data. SANS data were fit with a form factor for spherical micelles,[39-42] and details of this model are provided

in the Supporting Information. The reported errors for the SANS data modeling results were due to the uncertainty in solution concentration.

The corona profiles obtained from the SANS data modeling were rescaled using Equation 6,

$$\int 4\pi\widehat{\rho}_{corona}(r)r^2 d\ r = N_{agg}\nu_{corona} \quad (6)$$

in which $\widehat{\rho}_{corona}(r)$ is the rescaled corona profile and represents the volume fraction of the corona chains, r is the distance from the center of the micelles, N_{agg} is the aggregation number, and ν_{corona} is the volume of the PNIPAM block.[39, 40] The micelle radius was defined as the radius at which the volume fraction of PNIPAM in the corona profile was less than 0.02.[40, 41]

Results

The pincer CTA **2** was designed to facilitate end-functionalization of polymer chains with reactive centers for potential catalytic applications (see Scheme 1).[32] As shown in Scheme 1, RAFT agents can be readily coupled to the primary alcohol on pincer ligand **1**, allowing for the polymerization of a wide variety of monomers.[32, 48] In this work, we chose the RAFT agent S-dodecyl-S' -(α', α' -dimethyl-α'' -acetic acid) (DDMAT) for its ability to polymerize acrylamide monomers.[27] RAFT polymerization of NIPAM using CTA **2** produced a series of end-functionalized PNIPAM homopolymers, **3**, with controlled molecular weights and molecular weight distributions. The hydrophobic RAFT agent was removed from **3** to afford polymers functionalized only at the α-end by the pincer ligand, **4**.[28] The polymers examined in this study are summarized in Table 1.

Peaks associated with the hydrophobic pincer end-group were seen clearly in the ^{1}H NMR spectra (at δ = 3.7, 1.2, and 0.8 ppm, relative to TMS) in chloroform, a good solvent for both the end-group and the polymer (Figure 1). However in D_2O, a selective solvent for PNIPAM, the end-group peaks were attenuated. The attenuation of these peaks indicated that the end-group was confined to a less mobile environment and implied that the polymers self-assembled in D_2O.

The aqueous solution assembly of these polymers was further investigated by DLS and SLS. All scattering experiments were performed at concentrations much greater than the critical micelle concentration (CMC $\approx 10^{-2}$ mg mL^{-1}); therefore the concentration of unimers was negligible (see Figure S1). At all concentrations, the DLS results showed a major population of small micelles with hydrodynamic radii (R_H) of 10 -20 nm, and a minor population of larger aggregates, $R_H \sim 200$ nm (Figure S2, inset). The R_H values for the micelles (Table 2) were calculated according to the Stokes-Einstein equation, using the diffusion coefficient for the fast mode of relaxation extrapolated to zero concentration. As expected, the micelle radii increased with PNIPAM molecular weight.[49-52] The larger aggregates were not easily removed by filtration, changes in concentration, or by a variety of different preparation methods. However, the weight concentration of these large aggregates was negligible given that the scattered light intensity is proportional to the particle molecular weight and has a power law dependence on particle size (where the exponent is related to the shape of the scatterers). [53] Similar populations of large aggregates were reported for poly(ethylene oxide) (PEO) end-capped with dodecyl groups and were identified as spurious aggregates.[53]

To account for the presence of the larger aggregates in the SLS experiments, DLS and SLS data were collected simultaneously.[53-55] The relative scattered intensity contributions from the micelles (fast mode of relaxation) and larger spurious aggregates (slow mode of

relaxation) were determined from the DLS data, which allowed for the calculation of the Rayleigh ratio for the micelles only ($R_{\theta,fast}$) (see Experimental Section for additional details). Because the micelle radius of gyration (R_g) was less than 20 nm, $Kc/R_{\theta,fast}$ was independent of q (Figure S4) and an accurate R_g could not be determined using light scattering methods. However, the $Kc/R_{\theta,fast}$ values were averaged across the different q-values and plotted versus concentration to determine the micelle molecular weight (M_w) and second virial coefficient (A_2) (Figure S5). The micelle molecular weights were used to determine the aggregation number according to $N_{agg} = M_{w,micelle}/M_{w,polymer}$ (Table 2). The aggregation number decreased with increasing PNIPAM molecular weight, consistent with previous experimental literature and scaling theories for block copolymer assemblies.[49-52] Values for M_wA_2 ranged from -9.5 x10^{-4} to 9.3 x10^{-4} mL g $^{-1}$, which were several orders of magnitude smaller than typical values for polymeric micelles (~ 10^0 mL g^{-1} to 10^2 mL g_{-1}).[56-58] Interpreting M_wA_2 values for self-assembled systems often is complicated.[58, 59] Here, the small M_wA_2 values likely suggest minimal interactions between the micelles.

The solution assembly of sample 4c also was investigated using cryo-TEM. While polymeric coronas often are not visible in cryo-TEM due to their hydrated nature; the direct visualization of micelle coronas (including PNIPAM) has been reported previously.[36, 38, 56, 60-62] As seen in Figure 2, cryo-TEM further supported that the amphiphilic homopolymer formed spherical micelles in aqueous solutions. Moreover, assuming mass-thickness contrast dominates (i.e. small contribution from the phase contrast),[36, 63] the gray scale profile extracted from cryo-TEM micrographs should be related to the electron density profile of the micelles. The profile was fit assuming a radially decreasing density profile that was modeled as a linear combination of 2 b splines. This functional form for the corona profile gave a good fit to the gray scale profile and suggested that the micelle radius was ~ 20 nm, which was consistent with the light scattering results.

To further investigate the structural profile of the micelles, SANS experiments were performed on micelle solutions prepared in D_2O. The SANS data also were fit with a form factor model for spherical polymer micelles with a homogenous core and radially decreasing corona density profile, modeled as a linear combination of 2 b splines.[39, 40, 42, 64] Accounting for the corona density profile resulted in good fits to the SANS data, shown in Figure 3a. A slight upturn in the low-q data for sample 4a deviated from the model fit, suggesting there may be aggregates in solution as possibly indicated by the light scattering measurements. Similarly, Winnik *et al.*, reported an increase in scattered intensity at low-q upon heating their telechelic-PNIPAM flower micelles, which they fit with a model for micellar aggregates.[11] Here, accounting for the scattering contributions from micellar aggregates did not significantly affect the fit results for the individual micelles and therefore was not included while modeling the SANS data.

The results of the SANS data modeling are summarized in Table 2 and Figure 3b. The analysis suggested that the micelle core radius was between 1 and 2 nm, which was consistent with the length of a fully extended C_{12} chain.[65, 66] However, the fits were not sensitive to values within this range due to the small contribution of the core block to the overall scattered intensity. The micelle cores were surrounded by a diffuse, hydrated corona characteristic of star-like micelles, as seen in the corona profiles in Figure 3b. The micelle structure determined from the SANS data modeling also was qualitatively consistent with molecular simulations using dissipative particle dynamics (see Supporting Information for additional details). As expected, the R_g of the corona chains and overall micelle size increased with PNIPAM molecular weight (Table 2). Additionally, the SANS data suggested that the aggregation number decreased with increasing PNIPAM molecular weight, and this trend was consistent with the SLS results.

Discussion

The results presented here clearly indicate that the SCS pincer functionalized polymers self-assembled into well-defined micelles. Additionally, the amphiphilic homopolymers studied here followed trends similar to those reported for block copolymers. As seen in Table 2, all of the characterization results were in good agreement and indicated that the micelle radius increased with increasing N_{PNIPAM}. The overall size of star-like micelles, particularly those with small cores, depends on the dimensions of the hydrophilic block. Accordingly, the micelle radius, R, should scale with the degree of polymerization of the hydrophilic block, N_{philic}, as $R \sim N_{philic}^{\delta}$.[5, 52, 67] Fitting the data in Table 2 suggests that the N_{PNIPAM} scaling exponent for micelle radius is within the range of literature values for δ, with a value between 0.5 and 1.[49, 67] However; additional data points would be needed to definitively assign the scaling dependence, as these fits were based on only 3 samples. N_{agg} weakly decreased with increasing N_{PNIPAM} (Table 2), consistent with experimental studies of BCP micelles in which $N_{agg} \sim N_{philic}^{-\beta}$ and β ranged from 0.0 to 0.51.[49] Scaling theories for star-like BCP micelles also predicted that N_{agg} should weakly decrease, in a logarithmic fashion, with increasing N_{philic}.[52, 68]

Comparing the corona thickness to the root-mean-square end-to-end distance of PNIPAM in solution[69] suggests that the corona chains are moderately stretched in the micelles studied here (Table S3). Stretching of the corona chains has been reported for both amphiphilic homopolymer[66] and BCP micelles[49] and is attributed to the crowding and associated stretching of the chains near the micelle core. As indicated in Figure 3b, sample 4a has the highest polymer volume fraction near the core, corresponding to the most crowded and therefore the most stretched chains. Likewise, the degree of corona chain stretching increases with aggregation number (i.e., 4a > 4b > 4c), which is in agreement with trends reported for BCP micelles.[49] The extent of corona chain stretching for the amphiphilic homopolymer micelles is comparable to literature results for BCP micelles with similar aggregation numbers.[49]

Modeling the corona profile as a linear combination of 2 *b* splines resulted in good fits to both the cryo-TEM gray scale profile and the SANS data (Figures 2 and 3). Similarly, previous scattering studies of telechelic-PNIPAM[11] and hydrophobically-modified PEO[66, 70] also reported a radially decreasing corona profile. Though the corona profile extracted from cryo-TEM suggests that the corona chains extend to a smaller r than the profiles from SANS, the relative shape of the corona profiles was very similar, as illustrated by the normalized profiles in Figure 4. These results showed that corona profiles can be extracted from cryo-TEM micrographs, and highlighted the complementary use of scattering and cryo-TEM in the structural characterization of solution assemblies.

Conclusions

An SCS-pincer functionalized RAFT agent was used to synthesize a series of hydrophobically end-functionalized PNIPAM polymers that are promising precursors to solution-assembled nanoreactors. These amphiphilic homopolymers self-assembled into well-defined spherical micelles, in which the micelle radius, aggregation number, and corona density profile were dependent on the degree of polymerization of the PNIPAM block. To facilitate future investigations into the effects of nanoreactor structure on catalytic performance, the micelle structures were characterized thoroughly using DLS, SLS, cryo-TEM, and SANS. Importantly, detailed information about the micelle density profiles was extracted from the cryo-TEM micrographs and was comparable to the SANS result, highlighting the immense potential of the complementary use of these two techniques to characterize nanoscale solution-assemblies.

Supplementary Material

Refer to Web version on PubMed Central for supplementary material.

Acknowledgments

The EPSRC and University of Warwick are thanked for funding. Some equipment used in this research was funded by Birmingham Science City, with support from Advantage West Midlands and part funded by the European Regional Development Fund. T.H.E., M.O.S., R.P.M., and E.G.K. thank an Institutional Development Award (IDeA) from the National Institute of General Medical Sciences of the National Institutes of Health (NIH) grant, P20GM103541, for financial support. The statements herein do not reflect the views of the NIH. E.G.K. also acknowledges support from a Department of Defense, Air Force Office of Scientific Research, National Defense Science and Engineering Graduate (NDSEG) Fellowship, 32 CFR 168a. We acknowledge support of the National Institute of Standards and Technology (NIST), U.S. Department of Commerce for providing the neutron facilities used in this work. University of Delaware Center for Neutron Science (CNS) exploratory beam time was supported by NIST, U.S. Department of Commerce (#70NANB7H6178). We acknowledge the Keck Microscopy Facility at the University of Delaware for use of their TEM and Vitrobot.

References

1. Blanazs A, Armes SP, Ryan AJ. Macromol Rapid Commun. 2009; 30:267–277. [PubMed: 21706604]
2. Kelley EG, Albert JNL, Sullivan MO, Epps TH III. Chem Soc Rev. 201310.1039/C3CS35512H
3. Kim KT, Meeuwissen SA, Nolte RJM, van Hest JCM. Nanoscale. 2010; 2:844–858. [PubMed: 20648280]
4. Lazzari, M.; Lecommandoux, GLS. Block Copolymers in Nanoscience. Wiley-VCH; 2006.
5. Semenov AN, Joanny JF, Khokhlov AR. Macromolecules. 1995; 28:1066–1075.
6. Changez M, Kang NG, Lee JS. Small. 2012; 8:1173–1179. [PubMed: 22337611]
7. Kale TS, Klaikherd A, Popere B, Thayumanavan S. Langmuir. 2009; 25:9660–9670. [PubMed: 19453140]
8. Ringsdorf H, Venzmer J, Winnik FM. Macromolecules. 1991; 24:1678–1686.
9. Bathfield, Ml; Daviot, D.; D'Agosto, F.; Spitz, R.; Ladavière, C.; Charreyre, M-Trs; Delair, T. Macromolecules. 2008; 41:8346–8353.
10. Du J, Willcock H, Patterson JP, Portman I, O'Reilly RK. Small. 2011; 7:2070–2080. [PubMed: 21648072]
11. Koga T, Tanaka F, Motokawa R, Koizumi S, Winnik FM. Macromolecules. 2008; 41:9413–9422.
12. Hadjichristidis N, Pispas S, Pitsikalis M. Prog Polym Sci. 1999; 24:875–915.
13. Boerakker MJ, Hannink JM, Bomans PHH, Frederik PM, Nolte RJM, Meijer EM, Sommerdijk NAJM. Angew Chem. 2002; 41:4239–4241. [PubMed: 12434350]
14. Kujawa P, Segui F, Shaban S, Diab C, Okada Y, Tanaka F, Winnik FM. Macromolecules. 2006; 39:341–348.
15. Kujawa P, Tanaka F, Winnik FM. Macromolecules. 2006; 39:3048–3055.
16. Kujawa P, Watanabe H, Tanaka F, Winnik FM. Eur Phys J E. 2005; 17:129–137. [PubMed: 15880290]
17. Serero Y, Aznar R, Porte G, Berret JF, Calvet D, Collet A, Viguier M. Phys Rev Lett. 1998; 81:5584–5587.
18. Heldt N, Gauger M, Zhao J, Slack G, Pietryka J, Li Y. React Funct Polym. 2001; 48:181–191.
19. Kitano H, Akatsuka Y, Ise N. Macromolecules. 1991; 24:42–46.
20. Kitano H, Ishino Y, Yabe K. Langmuir. 2001; 17:2312–2316.
21. Li C, Hu J, Yin J, Liu S. Macromolecules. 2009; 42:5007–5016.
22. Xu JT, Tao L, Boyer C, Lowe AB, Davis TP. Macromolecules. 2011; 44:299–312.
23. de Paz Báñez MV, Robinson KL, Vamvakaki M, Lascelles SF, Armes SP. Polymer. 2000; 41:8501–8511.

24. Akiyoshi K, Kang EC, Kurumada S, Sunamoto J, Principi T, Winnik FM. Macromolecules. 2000; 33:3244–3249.
25. Renou F, Nicolai T, Nicol E, Benyahia L. Langmuir. 2009; 25:515–521. [PubMed: 19072147]
26. Greenland BW, Bird MB, Burattini S, Cramer R, O'Reilly RK, Patterson JP, Hayes W, Cardin CJ, Colquhoun HM. Chem Commun. 2013; 49:454–456.
27. Moad G, Rizzardo E, Thang SH. Polymer. 2008; 49:1079–1131.
28. Willcock H, O'Reilly RK. Polym Chem. 2010; 1:149–157.
29. Bai ZF, Lodge TP. Langmuir. 2010; 26:8887–8892. [PubMed: 20148546]
30. Cotanda P, Lu A, Patterson JP, Petzetakis N, O'Reilly RK. Macromolecules. 2012; 45:2377–2384.
31. Horton JM, Bai ZF, Jiang XM, Li DJ, Lodge TP, Zhao B. Langmuir. 2011; 27:2019–2027. [PubMed: 21189037]
32. Patterson JP, Cotanda P, Kelley EG, Moughton AO, Lu A, Epps TH III, O'Reilly RK. Polym Chem. 2013; 4:2033–2039. [PubMed: 23539324]
33. Cui H, Hodgdon TK, Kaler EW, Abezgauz L, Danino D, Lubovsky M, Talmon Y, Pochan DJ. Soft Matter. 2007; 3:945–955.
34. Danino D. Curr Opin Colloid Interface Sci. 2012; 17:316–329.
35. Weissman H, Rybtchinski B. Curr Opin Colloid Interface Sci. 2012; 17:330–342.
36. Crassous JJ, Rochette CN, Wittemann A, Schrinner M, Ballauff M, Drechsler M. Langmuir. 2009; 25:7862–7871. [PubMed: 19317419]
37. Ku TH, Chien MP, Thompson MP, Sinkovits RS, Olson NH, Baker TS, Gianneschi NCJ. Am Chem Soc. 2011; 133:8392–8395.
38. Zheng Y, Won YY, Bates FS, Davis HT, Scriven LE, Talmon YJ. Phys Chem B. 1999; 103:10331–10334.
39. Bang J, Viswanathan K, Lodge TP, Park MJ, Char KJ. Chem Phys. 2004; 121:11489–11500.
40. Kelley EG, Smart TP, Jackson AJ, Sullivan MO, Epps TH III. Soft Matter. 2011; 7:7094–7102.
41. Pedersen JS, Gerstenberg MC. Colloids Surf A. 2003; 213:175–187.
42. Pedersen JS, Svaneborg C, Almdal K, Hamley IW, Young RN. Macromolecules. 2003; 36:416–433.
43. Armarego, WLF.; Chai, CLL. Purification of laboratory chemicals. Butterworth-Heinemann: Oxford; 2003.
44. Berne, BJ.; Pecora, R. Dynamic light scattering, with application to chemistry, biology, and physics. Wiley; New York: 1976.
45. Jakes J. Collect Czech Chem Commun. 1995; 60:1781–1797.
46. Schneider CA, Rasband WS, Eliceiri KW. Nat Methods. 2012; 9:671–675. [PubMed: 22930834]
47. Kline SJ. Appl Crystallogr. 2006; 39:895–900.
48. Moughton AO, O'Reilly RK. J Am Chem Soc. 2008; 130:8714–8725. [PubMed: 18549205]
49. Forster S, Zisenis M, Wenz E, Antonietti M. J Chem Phys. 1996; 104:9956–9970.
50. Nagarajan R, Ganesh K. J Chem Phys. 1989; 90:5843–5856.
51. Pioge S, Fontaine L, Gaillard C, Nicol E, Pascual S. Macromolecules. 2009; 42:4262–4272.
52. Zhulina EB, Adam M, LaRue I, Sheiko SS, Rubinstein M. Macromolecules. 2005; 38:5330–5351.
53. Chassenieux C, Nicolai T, Durand D. Macromolecules. 1997; 30:4952–4958.
54. Lefay C, Charleux B, Save M, Chassenieux C, Guerret O, Magnet S. Polymer. 2006; 47:1935–1945.
55. Lejeune E, Chassenieux C, Colombani O. Prog Colloid Polym Sci. 2011; 138:7–16.
56. Colombani O, Ruppel M, Burkhardt M, Drechsler M, Schumacher M, Gradzielski M, Schweins R, Müller AHE. Macromolecules. 2007; 40:4351–4362.
57. Convertine AJ, Lokitz BS, Vasileva Y, Myrick LJ, Scales CW, Lowe AB, McCormick CL. Macromolecules. 2006; 39:1724–1730.
58. Khougaz K, Zhong XF, Eisenberg A. Macromolecules. 1996; 29:3937–3949.
59. Vagberg LJM, Cogan KA, Gast AP. Macromolecules. 1991; 24:1670–1677.

60. Betthausen E, Drechsler M, Fortsch M, Schacher FH, Müller AHE. Soft Matter. 2011; 7:8880–8891.
61. Synatschke CV, Schacher FH, Fortsch M, Drechsler M, Müller AHE. Soft Matter. 2011; 7:1714–1725.
62. Wolf A, Walther A, Müller AHE. Macromolecules. 2011; 44:9221–9229.
63. Langmore JP, Smith MF. Ultramicroscopy. 1992; 46:349–373. [PubMed: 1336234]
64. Choi SY, Bates FS, Lodge TP. J Phys Chem B. 2009; 113:13840–13848. [PubMed: 19320497]
65. Israelachvili, J. Intermolecular & Surface Forces. Second. Elsevier; 1991.
66. Sommer C, Pedersen JS, Garamus VM. Langmuir. 2005; 21:2137–2149. [PubMed: 15752000]
67. Halperin A. Macromolecules. 1987; 20:2943–2946.
68. Zhulina EB, Borisov OV. Macromolecules. 2012; 45:4429–4440.
69. Kubota K, Fujishige S, Ando I. Polym J. 1990; 22:15–20.
70. Beaudoin E, Borisov O, Lapp A, Billon L, Hiorns RC, Francois J. Macromolecules. 2002; 35:7436–7447.

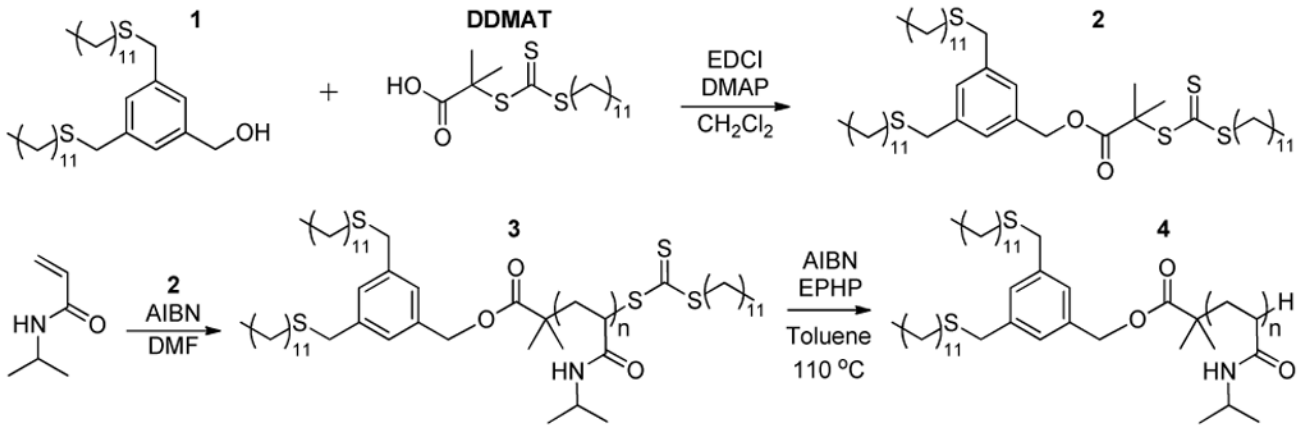

Scheme 1.

Synthesis of SCS-pincer functionalized RAFT agent[a] and end-functionalized PNIPAM polymers[b]

[a](Top) Coupling of a pincer alcohol, **1**, with DDMAT to form an SCS-pincer functionalized RAFT agent, **2**.[b](Bottom) Polymerization of NIPAM to form a telechelic polymer, **3**, followed by RAFT end-group removal to generate a mono-functionalized homopolymer, **4**.

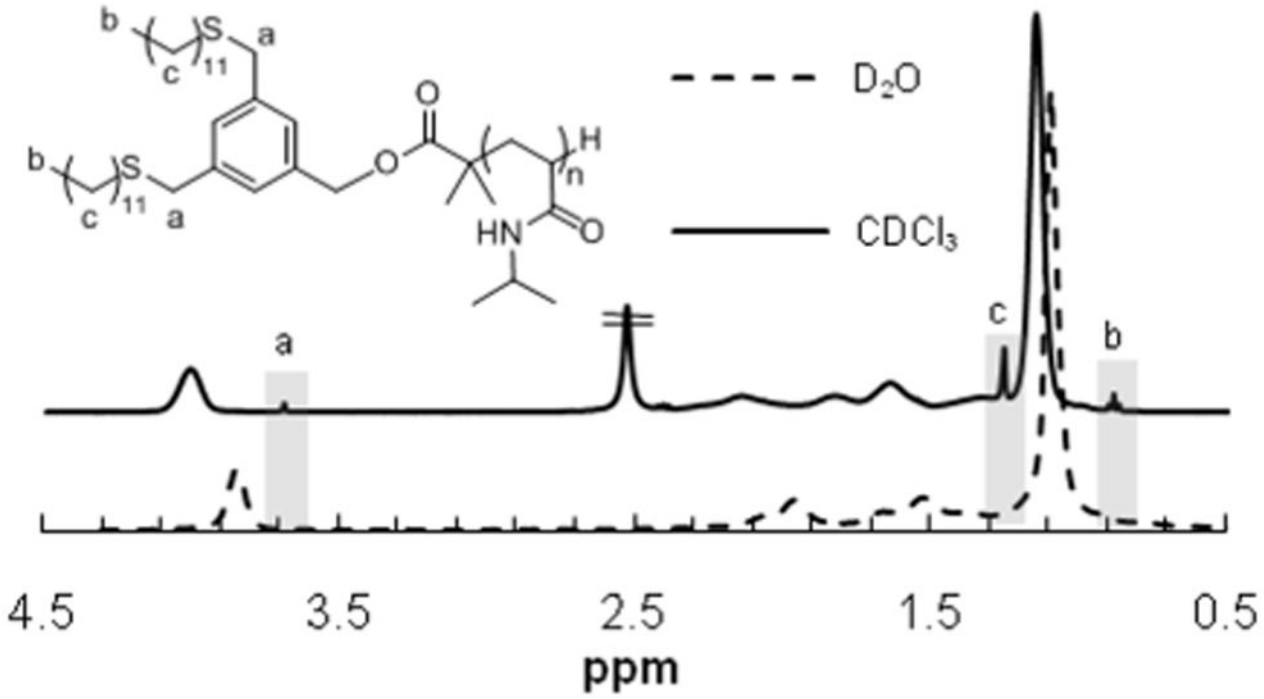

Figure 1.
^{1}H NMR spectra of 4b in $CDCl_3$ and D_2O, in which boxed regions highlight the peaks associated with hydrophobic pincer end-group. The end-group peaks were attenuated in D_2O due to polymer self-assembly.

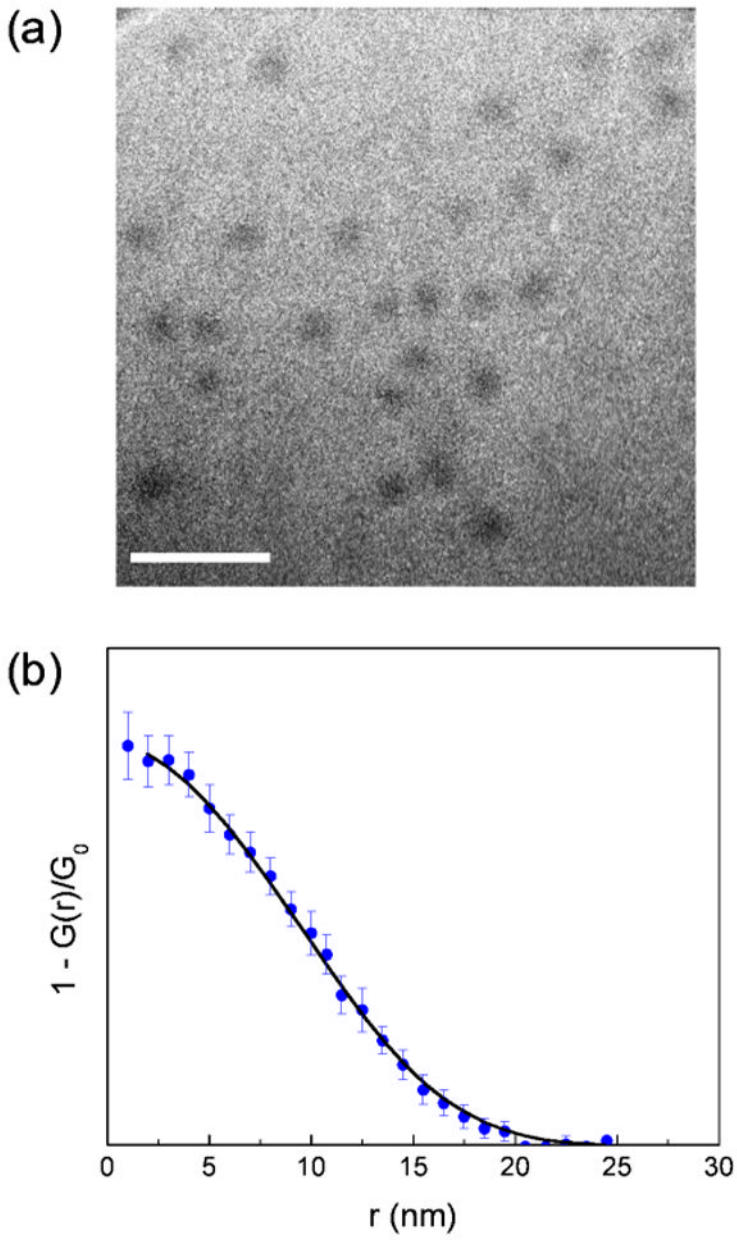

Figure 2.
(a) Cryo-TEM micrograph and (b) corresponding gray scale profile from cryo-TEM micrograph analysis and fit for sample 4c, supporting the PNIPAM chains form a diffuse, hydrated corona. Contrast shown in (a) was enhanced by 5% in ImageJ for clarity; the contrast was not adjusted for the profile analysis. Scale bar is 100 nm. The gray scale profile in (b) was averaged over 50 micelles.

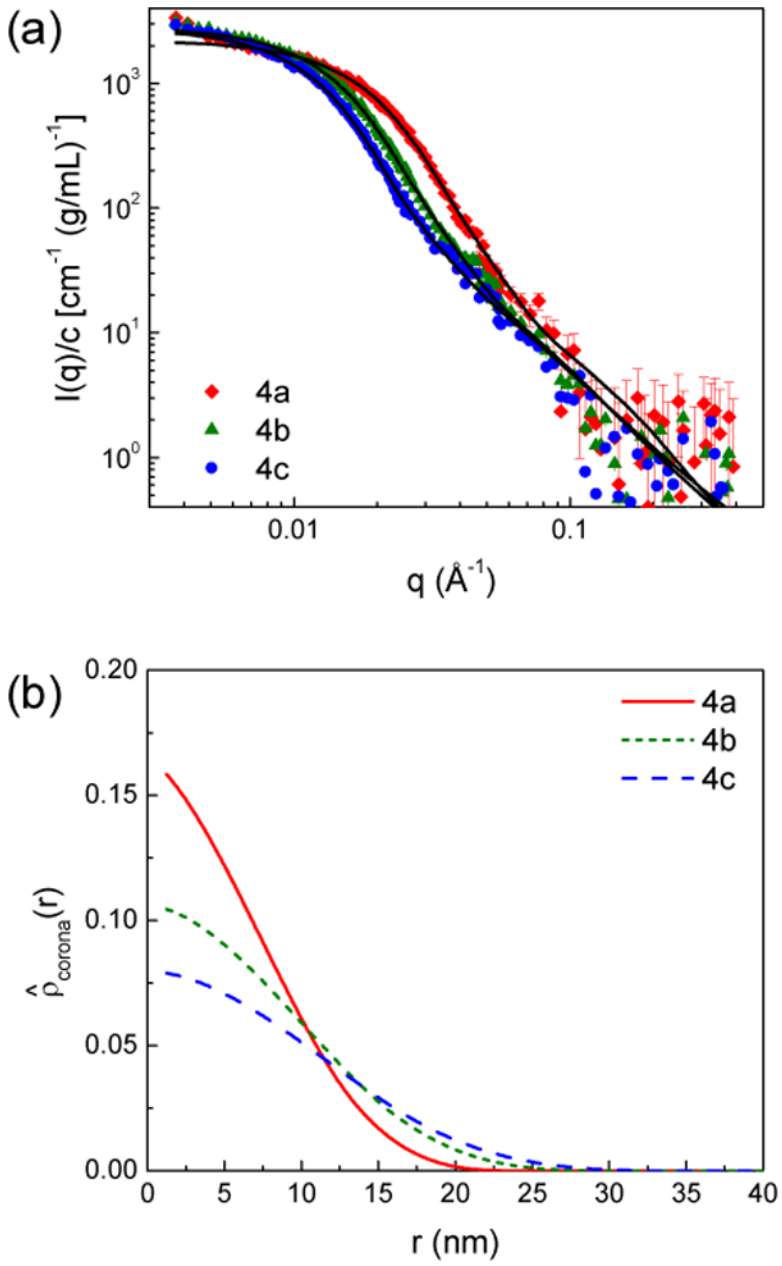

Figure 3.
(a) SANS data (symbols) and fits with a spherical micelle form factor (lines) for 4a, 4b, and 4c in D_2O and (b) micelle corona profiles from the SANS data fits.

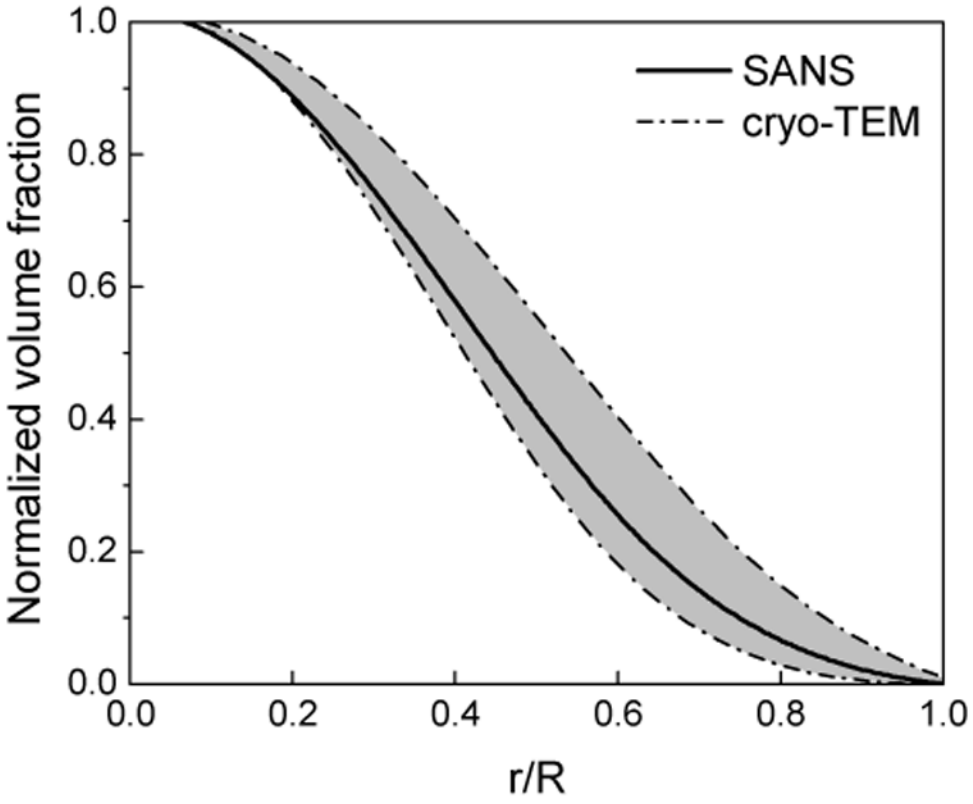

Figure 4.
Comparison of normalized corona profiles for sample 4c from cryo-TEM micrograph analysis and SANS data modeling. Shaded area represents the range of dimensionless volume fraction profiles that gave similar fits to the gray scale profile from cryo-TEM. Solid line is the dimensionless profile from the SANS data modeling. R is the radius at which the respective corona profile decreased to 0.

Table 1

Polymer characterization data

Sample	M_n [a] (kDa)	M_n [b] (kDa)	M_w [c] (kDa)	N_{PNIPAM} [d]	Đ [a]	$f_{hydrophobic}$ [e]
4a	11.8	14.2	15.8	120	1.12	0.04
4b	20.3	21.0	25.3	180	1.21	0.03
4c	23.8	30.6	38.5	270	1.24	0.02

[a] From SEC based on poly(methyl methacrylate) standards.

[b] Based on end-group analysis from ^{1}H NMR.

[c] Calculated from ^{1}H NMR and SEC according to $M_W = (N_{PNIPAM}M_O + M_{pincer}) * Đ$.

[d] Degree of polymerization of PNIPAM block from ^{1}H NMR end-group analysis.

[e] Hydrophobic weight fraction calculated from ^{1}H NMR.

Table 2

Summary of micelle characterization data

Sample	R_H (nm)	R (nm)	R_G,corona (nm)	N_{agg}	N_{agg}
	DLS	SANS	SANS	SLS	SANS
4a	11 ± 1	15 ± 1	4.5 ± 0.9	54 ± 5	48 ± 2
4b	15 ± 2	17 ± 1	5.1 ± 0.4	40 ± 4	43 ± 2
4c	22 ± 2	18 ± 1	6.2 ± 0.5	36 ± 4	34 ± 3